Article

A novel in vivo platform for studying alveolar bone regeneration in rat

Journal of Tissue Engineering
4: 2041731413517705

DOI: 10.1177/2041731413517705
tej.sagepub.com
SAGE

Joong-Hyun Kim[1,2], Ho-Jin Moon[2,3], Tae-Hyun Kim[1,2], Jong-Min Jo[1,2], Sung Hee Yang[1,2], Deboki Naskar[4], Subhas C Kundu[4], Wojciech Chrzanowski[2,5], and Hae-Won Kim[1,2,6]

Abstract

Alveolar bone regeneration is a significant challenge in dental implantation. Novel biomaterials and tissue-engineered constructs are under extensive development and awaiting in vivo animal tests to find clinical endpoint. Here, we establish a novel in vivo model, modifying gingivoperiosteoplasty in rat for the alveolar bone regeneration. Rat premaxillary bone defects were filled with silk scaffold or remained empty during the implantation period (up to 6 weeks), and harvested samples were analyzed by micro-computed tomography and histopathology. Empty defects showed increased but limited new bone formation with increasing implantation period. In defects implanted with silk sponge, the bone formation was significantly greater than that of empty defect, indicating an effective role of silk scaffold in the defect model. The modified premaxillary defect model in rat is simple to perform, while mimicking the clinical conditions, finding usefulness for the development of biomaterials and tissue-engineered constructs targeting alveolar bone regeneration in dental implantation.

Keywords

Animal model, silk, rat alveolar bone, bone regeneration, dental implantation

Received: 4 September 2011; accepted: 2 December 2013

Introduction

Maxillary and mandibular bone surrounds and supports tooth structure, but it can be destroyed by several factors including acquired injury, congenital disorders, tumors, infections, and tooth loss.[1] Repair of such bone loss is a major challenge in oral and maxillofacial care, especially for the aged population because of their decreased ability for bone repair. This has brought about a number of investigations of the regeneration or repair of bone defects.[2,3] A variety of techniques are used in the clinic for alveolar bone regeneration, such as osseous grafts using scaffolds or guided bone regeneration using membranes.[2,4,5] However, it is difficult to repair large defects, mainly due to donor-site morbidity, graft resorption, host disease transmission, immune responses, and a limited ability for new bone formation.

Bone tissue engineering offers a promising alternative treatment option for the regeneration of alveolar bone. A variety of candidate biomaterials are proposed to populate stem and progenitor cells to induce osteogenesis and to consequently achieve tissue-equivalent constructs.[1,6–8] Clearly, there is a growing demand for the development of tissue-engineering components and techniques that are clinically available to completely regenerate alveolar bone defects.

Many animal models have also been developed for alveolar bone grafting.[9–14] Animal study for testing

[1]Institute of Tissue Regeneration Engineering (ITREN), Dankook University, Cheonan, Republic of Korea
[2]Department of Nanobiomedical Science & BK21 PLUS NBM Global Research Center for Regenerative Medicine, Dankook University, Cheonan, Republic of Korea
[3]Department of Conservative Dentistry, Dankook University Dental College, Cheonan, Republic of Korea
[4]Department of Biotechnology, Indian Institute of Technology Kharagpur, Kharagpur, India
[5]Faculty of Pharmacy, The University of Sydney, Sydney, NSW, Australia
[6]Department of Biomaterials Science, Dankook University Dental College, Cheonan, Republic of Korea

Corresponding author:
Hae-Won Kim, Institute of Tissue Regeneration Engineering (ITREN), Dankook University, Cheonan, 330-714, Republic of Korea.
Email: kimhw@dku.edu

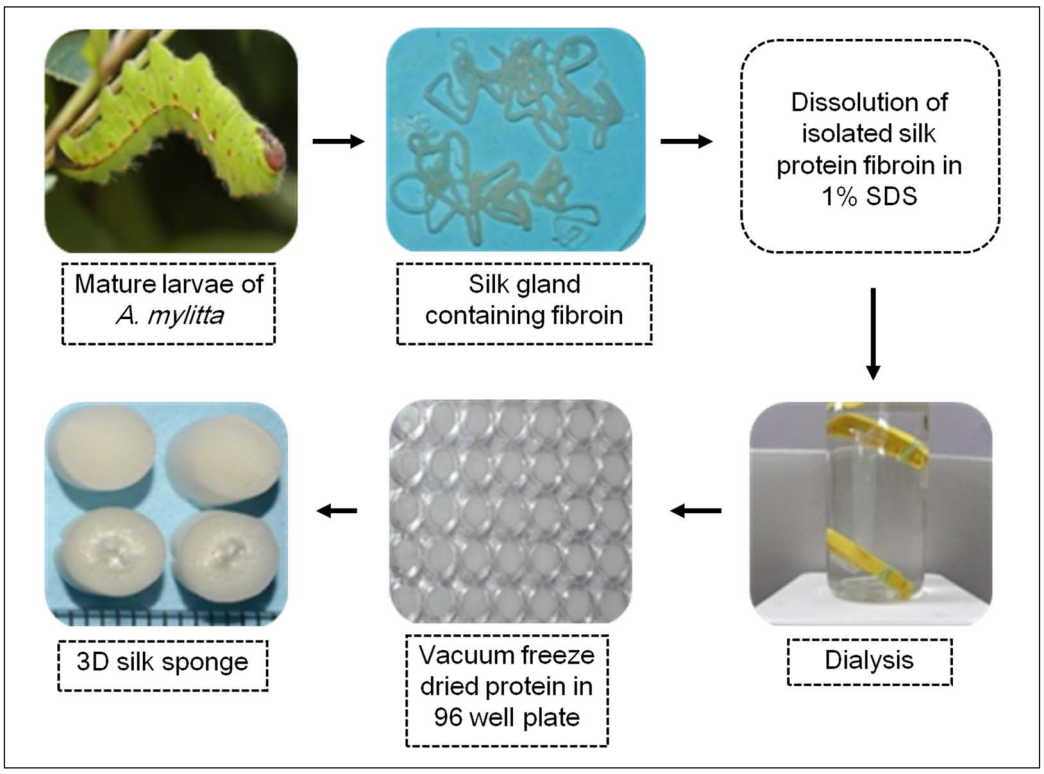

Figure 1. Fabrication method of 3D sponges from nonmulberry silk protein fibroin.
3D: three-dimensional; SDS: sodium dodecyl sulfate.

biomaterials and tissue-engineered constructs is essential because it is difficult to extrapolate in vitro research data to in vivo results without relevant and well-characterized models.[1] Although many animal models have been developed to advance techniques and screen candidate grating materials, in vivo models using small animals have been limited. One major reason for this is the difficulty in manipulation and surgical operation of defects of a reduced anatomical size.[15–17] Obviously large animal models are favored from a clinical perspective, but these animals are more expensive to purchase and maintain and are generally considered only for preclinical studies.[6,18] Critical-sized defect models of the rodent skull have been widely used as the first stage of in vivo study for bone regeneration, but the alveolar bone defect model better represents clinical situations where alveolar bone regeneration is required (such as sinus lifting and dental implantation). The use of rats in an alveolar defect model is relatively limited in use, mainly due to the difficulty of the surgical approach in the intraoral regions. An alveolar defect model in rats could save costs in the research and development of tissue-engineered constructs.

This study developed a rat alveolar bone defect model using a modified surgical technique, which is known as a gingivoperiosteoplasty (GPP) technique. This model provides an in vivo platform for researchers to develop biomaterials and tissue-engineered constructs that target alveolar bone regeneration for dental implantation and sinus lifting. The development of this small animal model could be capable of economically and rapidly representing clinical conditions and enabling the performance assessment of biomaterials and tissue-engineered constructs.

Materials and methods

Animal

The maxillary alveolar bone healing effect of three-dimensional (3D) silk sponge scaffold was determined in vivo using the rat maxillary defect model. The housing, care, and experimental protocol were approved by the Institutional Animal Care and Use Committee, Dankook University Korea. A total of eight, 11-weeks-old, 350–400 g healthy male Sprague-Dawley rats were included in this study.

Fabrication of 3D sponges from nonmulberry silk protein fibroin

The silk scaffolds were fabricated according to the method depicted in the Figure 1. In brief, crude silk protein fibroin was first isolated from the silkglands of nonmulberry (*Antheraea mylitta*) mature fifth instar larva, grown in the farm of Indian Institute of Technology, Kharagpur, according to the protocol described elsewhere.[19] The isolated protein was dissolved in 1%

sodium dodecyl sulfate (SDS) containing 10 mM Tris (pH 8.0) and 5 mM ethylenediaminetetraacetic acid (EDTA). The solution was then taken in a 12-kDa cellulose dialysis membrane and dialyzed against deionized water for 8 h with frequent water change.

For scaffold fabrication, 2% regenerated silk fibroin solution was cast on tissue culture well plates (96 wells) and immediately placed in −20°C for 24 h. Plates were then placed inside a vacuum freeze drier for another 24 h to dry the frozen protein solution, which produced highly porous 3D scaffolds. Scanning electron microscopy study showed that the pore size was usually uniform throughout the scaffold (110 ± 25 μm) as measured through ImageJ software,[20,21] and the porosity of the scaffolds was calculated to be approximately 97%.[22] The prepared silk scaffolds were treated with 70% ethanol for 15–20 min under ultraviolet light and were washed thoroughly with sterilized phosphate-buffered saline (PBS) inside the laminar hood.

Surgical procedures and experimental design

During the surgical operation, the animals were anesthetized with intramuscular injections of 80 mg/kg Zoletil and 10 mg/kg xylazine in the right quadriceps muscle. Epinephrine with 0.5% lidocaine was locally injected into gingival tissues of the premaxilla to decrease pain and bleeding during operation. Animals were placed in dorsal recumbency, and the operation field was prepared in the standard manner for aseptic surgery, using 10% povidone iodine and 70% ethyl alcohol. All instruments were sterilized prior to procedures, and all the surgical procedures on animals were carried out under general anesthesia using sterile techniques.

Following an incision through the palatal gingival epithelium using a 10 blade with a bard-parker scalpel, the underlying maxillary alveolar bone of the premaxilla was exposed (Figure 2(a) and (b)). A surgical trephine bur was used to create a standardized, semicircular defect 4 mm in diameter at the center region of the upper incisor socket, between the anterior and posterior inner margins of the incisor teeth on the lateral surface of each premaxilla bone. While using the bur, copious irrigation was done with cooled sterile isotonic saline. The defect was either left empty or filled with the trialed 3D silk sponge (Figure 2(c) and (d)). Two defects were created in each animal (Figure 2(e)), and the animals were assigned to four groups—Group A: empty defect with 2 weeks healing; Group B: empty defect with 4 weeks healing; Group C: empty defect with 6 weeks healing; and Group D: silk scaffold with 6 weeks healing (Figure 2(f)).

After the delivery of samples, the mucosal flaps were closed with a simple interrupted suture pattern using 4-0 absorbable suture (Figure 3(a)). After surgery, the rats were housed individually in cages at 20°C–24°C and 30%–70% relative humidity and were kept on a 12 h light/12 h dark cycle. Animals were maintained on a ground pellet food with standardized diet and water *ad libitum*. Animals were monitored for signs of infection, inflammation, and adverse effects by visual observation during study periods. The animals were sacrificed prior to harvesting the samples and surrounding tissues at 2, 4, and 6 weeks after surgery (Figure 3(b)).

Micro-computed tomographic analysis

The specimens were harvested from each animal at 2, 4, and 6 weeks postoperatively and were fixed in 10% neutral buffered formaldehyde solution for at least 24–48 h (Figure 3(c) and (d)). The samples were imaged using an in vivo high-resolution micro-computed tomography (μ-CT) system (Skyscan 1176; Skyscan, Aartselaar, Belgium) to evaluate tissue recovery and bone regeneration. The harvested samples were scanned by a camera with a pixel size of 12.56 μm, and a frame was achieved using a 1-mm aluminum filter, with a rotation step of 0.5°and a rotation angle of 180°. The X-ray was operated at a voltage of 65 kV, a current of 385 μA, and an exposure time of 279 ms. Approximately 400 scan slices per sample with an image pixel size of 17.93 μm were taken, and serial coronal-oriented tomograms were reconstructed from the raw images in the NRecon μ-CT Skyscan reconstruction software. A semicircular region of interest (ROI) was precisely positioned over each defect for quantitative analyses, encompassing all new bones within the defect site. Coronally oriented μ-CT images were then reformatted in an axial orientation. Reconstructed images over the ROI using CTAn Skyscan software were used to analyze bone formation and 3D images were created. Four samples for each group were measured and percentages of new bone volume (%), bone surface (mm^2), and bone surface density (1/mm) of newly formed bone within each ROI were measured by assigning a threshold for total bone content (including trabecular and cortical bone).

Histopathological analysis

After μ-CT scanning, specimens were decalcified in RapidCal sol (BBC, USA) and dehydrated in a graded series of increasing ethanol concentrations (from 70% to 100%). Then, they were bisected into anterior and posterior sections at the center of the defect and embedded in paraffin. Tissue cross-sections in the coronal plane, 5-μm-thick, were prepared perpendicularly to the cranial bone. The sections were placed on a slide glass and were stained with hematoxylin and eosin (H&E) stain using standard techniques for histopathological examination to check the biocompatibility and bone formation. Digital images were obtained under a light microscopy (IX71; Olympus, Tokyo, Japan) using Meta-Morph. Results of new bone formation within the defect were taken under 40x and 400x magnifications.

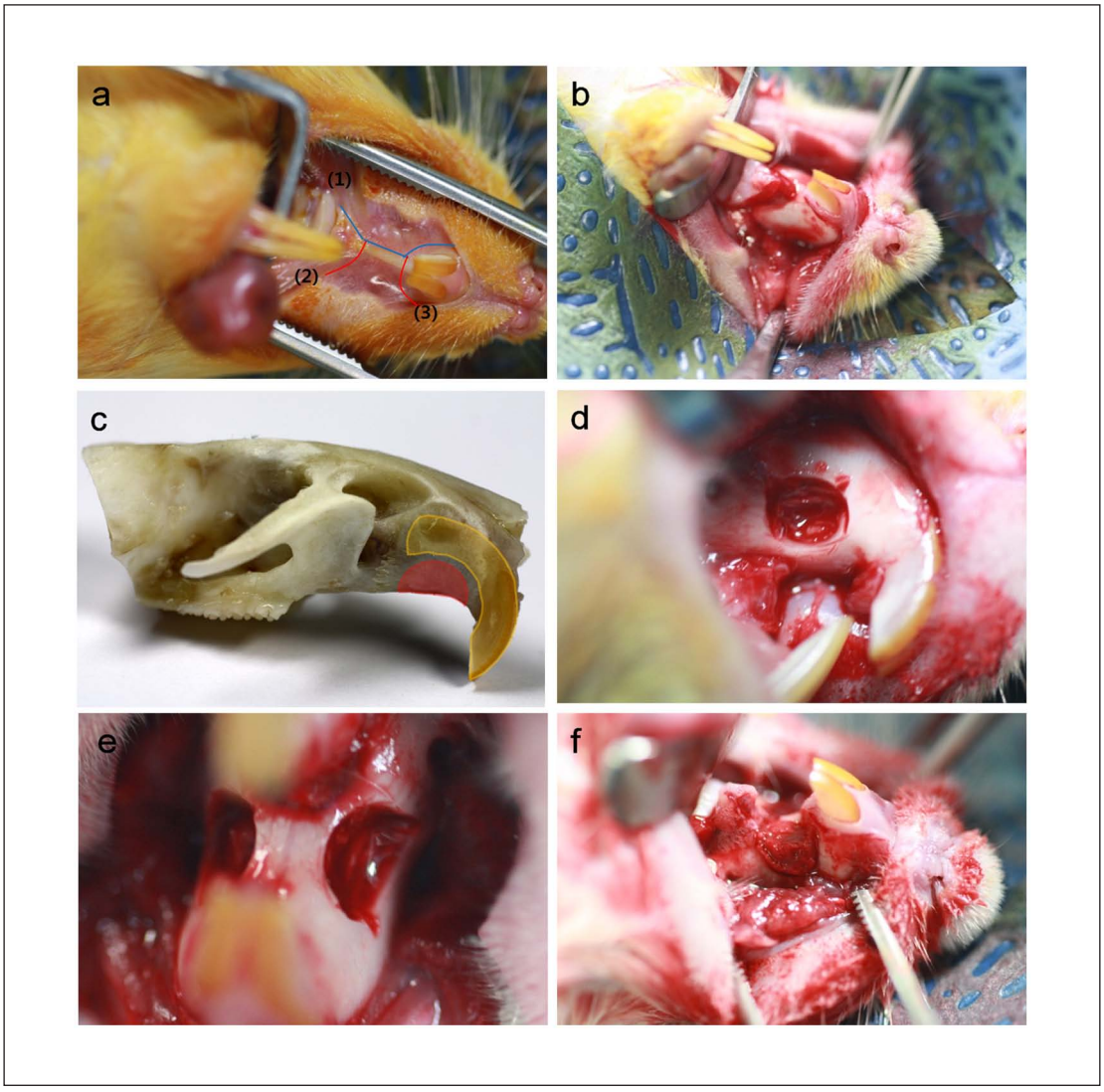

Figure 2. Photographs of rat premaxillary operation field. Note the dimensions of the defect used to produce standardized 4-mm-diameter semicircular defects. (a) Following an *x*-shape incision through the palatal gingival epithelium, (b) the underlying maxillary alveolar bone was exposed. (c and d) A 4-mm-diameter semicircular defect was created at the center region of the upper incisor socket, between the anterior and posterior inner margins of incisor teeth, on the lateral surface of each premaxilla bone. (e) Two defects were created on one animal and (f) were filled with silk scaffolds.

Statistical analysis

All data are presented as mean ± standard deviation. Differences between defect groups were assessed by analysis of variance (ANOVA). The comparison of Groups C and D used the Student's *t*-test. P values < 0.05 were considered significant.

Results

Surgical procedures and animal observation

A total of eight animals were analyzed for bone regeneration using the rat maxillary alveolar bone defect model. The operative procedure was well tolerated by all animals with no mortalities occurring during the animal's healing periods. The whole procedure, from palatal gingival epithelium incision to closure, was approximately 20–30 min per animal. No specific care was required postoperatively, and animals were able to eat without difficulty after 2 days. Throughout the study period, animals showed normal activity within 1 day of operation, a good healing response without adverse tissue reactions, and gained weight. Growth of the maxillary incisors was also not interrupted by modified GPP in all animals throughout the duration of the study. While harvesting the maxillary part of the control group skull, it was obvious that fibrous tissue had invaded the empty defect area (Figure 3(c)). The implanted silk scaffolds remained stable within the defect area throughout the study periods, and no visible fibrous invasion was detected. There was no gap between the

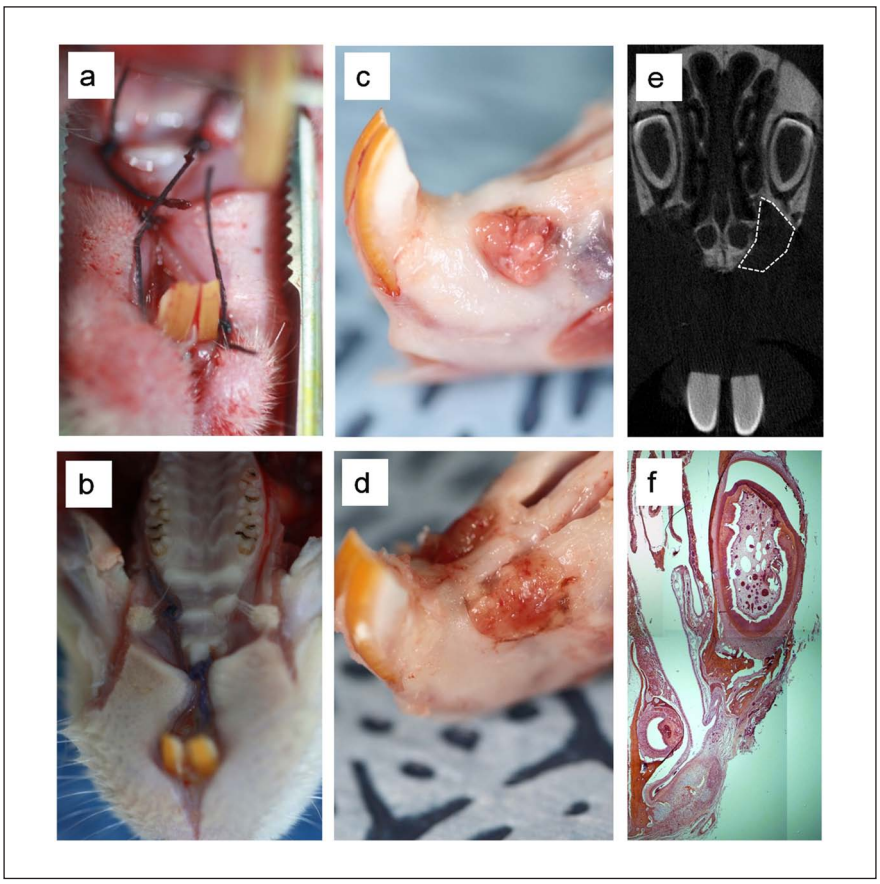

Figure 3. Photographs of rat premaxillary operation field, (a) after suture and (b) after sacrifice. Throughout the study period, animals showed a good healing response without adverse tissue reactions. (c and d) Harvested specimens of rat maxilla, with and without silk scaffold inserts, 6 weeks after surgery. (c) Defect without scaffold shows fibrous tissue invasion into the defect area, (d) but the defect implanted with scaffold shows no invasion. There were no visible signs of internal inflammation on harvested tissues. (e) Three-dimensional micro-computed tomographic images of a rat maxilla where silk scaffold was used to the defect (white dot line). The original outline of the 4-mm defect is clear. (f) Representative histology image of H&E staining of premaxillary area with the defect at 2 weeks. H&E: hematoxylin and eosin.

scaffold and the edge of the native bone, and there were no visible signs of internal inflammation on the harvested tissues (Figure 3(d)).

μ-CT analysis

Samples, including scaffolds and surrounding tissues, were imaged and analyzed using high-resolution μ-CT, and 2D and 3D images were constructed for four groups (Figure 4). μ-CT examination provided evidence that only minimal bone healing occurred in the empty defect group at 2 weeks post operation. However, bone formation increased in the empty defect group over time. For the silk scaffold group, substantial bone formation was evidenced, which was noticeably higher than that of the empty defect group at 6 weeks. Based on the images, a level of hard tissue formation occurred from the defect margin to the central region in the empty defect but the defect recovery was substantially limited, which, however, considerably improved when the scaffold was implanted.

Morphometric analyses of the μ-CT images were used to quantify the percent total bone volume, bone surface area, and the surface density, as presented in Figure 5. The empty defect showed a gradual increase in percent total bone volume with time (3.82% ± 0.2% at 2 weeks, 17.15% ± 2.09% at 4 weeks, and 27.28% ± 9.2% at 6 weeks) (Figure 5(a)). Moreover, Group IV showed significantly increased bone volume (49% ± 9.56%) compared to Group III. While the bone surface area of the silk scaffold also increased significantly (28.98 ± 5.88 mm^2 in Group III vs 64.89 ± 7.46 mm^2 in Group IV) (Figure 5(b)), the surface density level was not significantly increased (Figure 5(c)).

Histopathological analysis

New bone formation in the rat alveolar bone regeneration model was evaluated histopathologically under a light optical microscope using H&E staining. All three empty groups showed cell and/or tissue in-growth within the

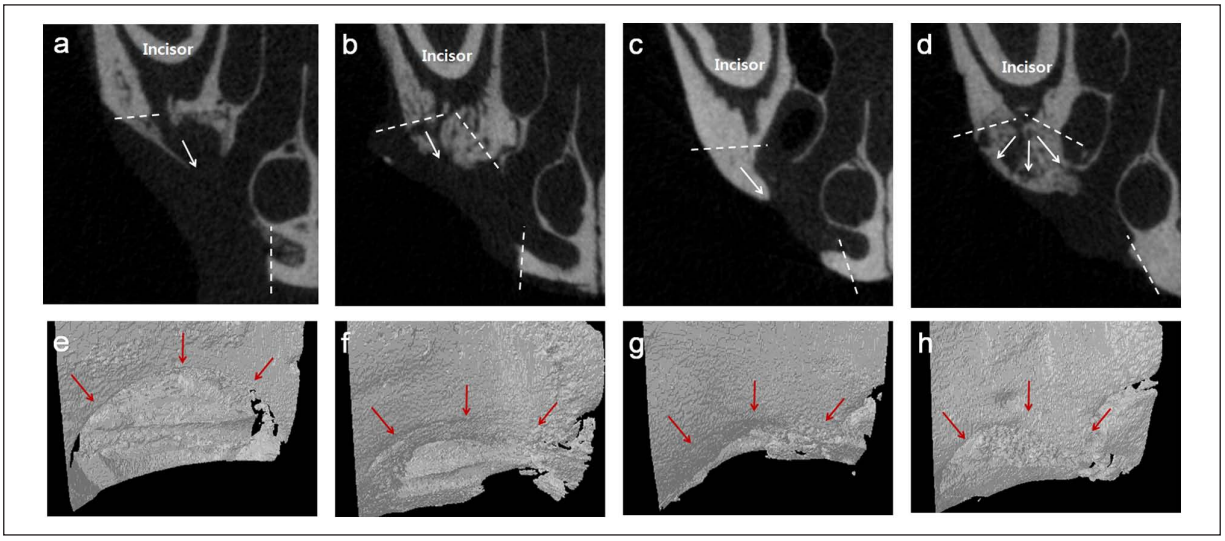

Figure 4. (a–d) 2D and (e–h) 3D micro-computed tomographic images, displaying new bone and defect area on (a and e) 2 weeks, (b and f) 4 weeks, and (c and g) 6 weeks of defect group and (d and h) 6 weeks of silk-implanted group. Note the increased bone formation in defects over time, and the improved growth at 6 weeks for the silk-implanted group. (a–d—white dot line: defect margin, white arrow: bone growing direction; e–h—red arrow: defect margin).

defect region, with increasing bone formation over time, but the defect was not completely regenerated with newly formed bone after 6 weeks (Figure 6(a)–(c)). The empty defect group at 2 and 4 weeks showed the formation of very thin and loose connective tissues with a limited amount of new bone formation in the defect (Figure 6(a) and (b)). At 6 weeks, better bone formation was apparent, but the loose nature of the connective tissues could still be observed (Figure 6(c)). Compared to the empty defect group, the silk scaffold group showed considerably improved new bone formation and good biocompatibility, with no significant inflammatory reaction (Figure 6(d)). New bone in-growth was well developed throughout the pore channels of the scaffold, showing an effective scaffolding role in osteoconduction. At higher magnification (Figure 6(e) and (f)), the newly formed bone in the silk scaffold group was mature and compact with a lining of osteoblasts, confirming the lamellar-structured woven bone, which was in contrast to that of the empty defect group, where the bone tissue was loosely organized as nonwoven bone. The scaffold pore surface was in direct contact with the newly formed bone without interposition of connective tissues.[23,24]

Discussion

For successful dental implantation, securing qualified bone levels in alveolar regions is essential, so substantial efforts have been made to augment and regenerate bone tissues in those areas.[25] Many surgical techniques have tried to get effective results, and scaffolding materials and tissue-engineered constructs have also been developed to provide an effective means for clinical therapies. Prior to clinical trials, such biomaterials and tissue-engineered constructs must be applied to in vitro cell experiments and in vivo animal models.

In fact, a variety of animal models for this alveolar bone healing have been demonstrated. The most common model is the calvarium defect model, which does not accurately mimic alveolar bone defects, particularly those requiring sinus lifting and dental implantation. Here, we focused on alveolar bone defect models, particularly GPP, in order to mimic a clinically available therapy. GPP is one of the commonly used surgical options for closure of the alveolar cleft, which requires closure of the nasoalveolar fistula and obliteration of the cleft with viable bone.[9,10,16,23,26,27] While GPP is widely used clinically, GPP animal models have received relatively little attention, mostly related to using large animals.

Thus, we developed a premaxillary bone defect animal model by modifying GPP using rats. Compared to large animals, small animals (particularly rodents like rats and mice) have economical, ethical, and technical merits.[18,28,29] Rodents are hygienic (specific pathogen-free (SPF) animal) and cheap and commonly used for bone regeneration models, such as long bone and calvarial models.[30] However, the operation and manipulation skills of small animals related with anatomical size are specially needed to develop models in small animals. Because of the small opening of a rat mouth, it is difficult to approach the oral region to create bone defects of consistent volume in the maxillary area.

In this study, we applied a defect which represents a alveolar bone defect in the rat to establish an appropriate and easy preclinical operation platform for bone

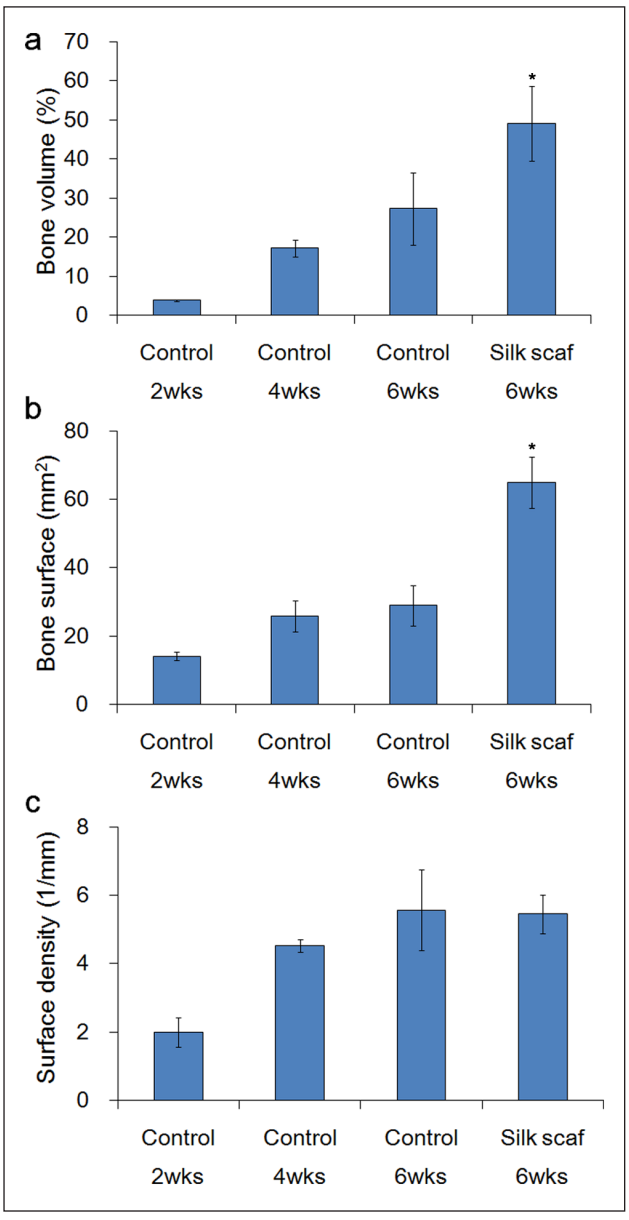

Figure 5. Image analyses of bone regeneration in premaxillary defects after 6 weeks of healing. Micro-computed tomographic images were analyzed for each defect at each time point. Graphs display the (a) percent volume of new bone, (b) bone surface area, and (c) bone surface density. *p < 0.05, by Student's *t*-test for n = 3.

regeneration in the dental implantation area. Previously, most surgical procedures made one bone defect with one incision and two bone defects with two incisions for premaxillary bone defect model.[15,16] However, because of the bleeding from the soft tissue of the defect area, it is not easy to make reproducible defects in the same location without damaging the underlying upper incisor teeth and surrounding alveolar tissues. In this study, we made a large *x*-shape incision to represent the two defects, which alleviated this damage. Drilling procedures to produce bone defects were also simplified by using a trephine bur. Previously, bone defects on the premaxillary region were made using a round bur, and the shape of defects were mostly square or rectangular. In this case, generation of the same-sized defects in the same place was not easy. The current method of creating large *x*-shape incisions while using the trephine bur enabled the creation of a representative defect in the same place with a reproducible size and quality. Operators must be able to distinguish the alveolar socket from the surrounding bone tissue because it has a grove, facilitating one to accurately position the trephine bur before drilling.

Sixteen defects were made in eight rats and 2 defects invaded the alveolar socket. One invasion affected the incisor, but the other did not destroy normal structure and did not interrupt the normal growth of upper incisor structures. It only affected a small part of the periodontal ligament and alveolar bone. One incisor showed a little grinding of the dentin by the trephine bur, but in this case, reparative dentin formation, periodontal ligament, and alveolar bone regeneration around the incisor were obvious. Except these two incisors, all other samples had intact periodontal tissue and incisors, suggesting that our premaxillary bone defect model has good reproducibility. Because our premaxillary bone defect model does not affect maxillary incisors or related periodontal structures, operators do not need to worry about unexpected damage that can prevent abnormal growth of the incisors. Oronasal communication is generally considered as a congenital problem, but it is also possible after the repair of premaxillary deficiency. It is defined as a failure of healing or a breakdown in the primary surgical repair of the palate.[31] We artificially created a bone defect on the premaxilla, which resulted in a communication between oral and nasal cavities. After the implantation of a silk scaffold, the mucosal flaps were closed with a simple interrupted suture pattern to achieve a total closure of the premaxilla. An ideal and successful premaxillary repair depends on a palatal gingival closure without tension.[32] After 6 weeks healing, there were no complications such as fistulas or dehiscence in the area of the implanted site. Our premaxillary bone defect model modifying GPP with the *x*-shape mucosal flap is thus considered to be a safe and easy operation.

Above all, since the major reason we develop this animal model is to test new biomaterials or tissue-engineered constructs for alveolar bone, it is of note to consider that our model is suitable for scaffold placement in the defect space and that a stable scaffold fixation with no migration was observed in all tested samples.

The efficacy of the current model was demonstrated over time (2, 4, and 6 weeks) using an empty defect group as a control as well as a silk scaffold experimental group. The silk scaffold, used herein as the experimental group, has previously been demonstrated to improve osteoblast proliferation and differentiation and to have good tissue compatibility.[33–35] In this study, it was considered to be a

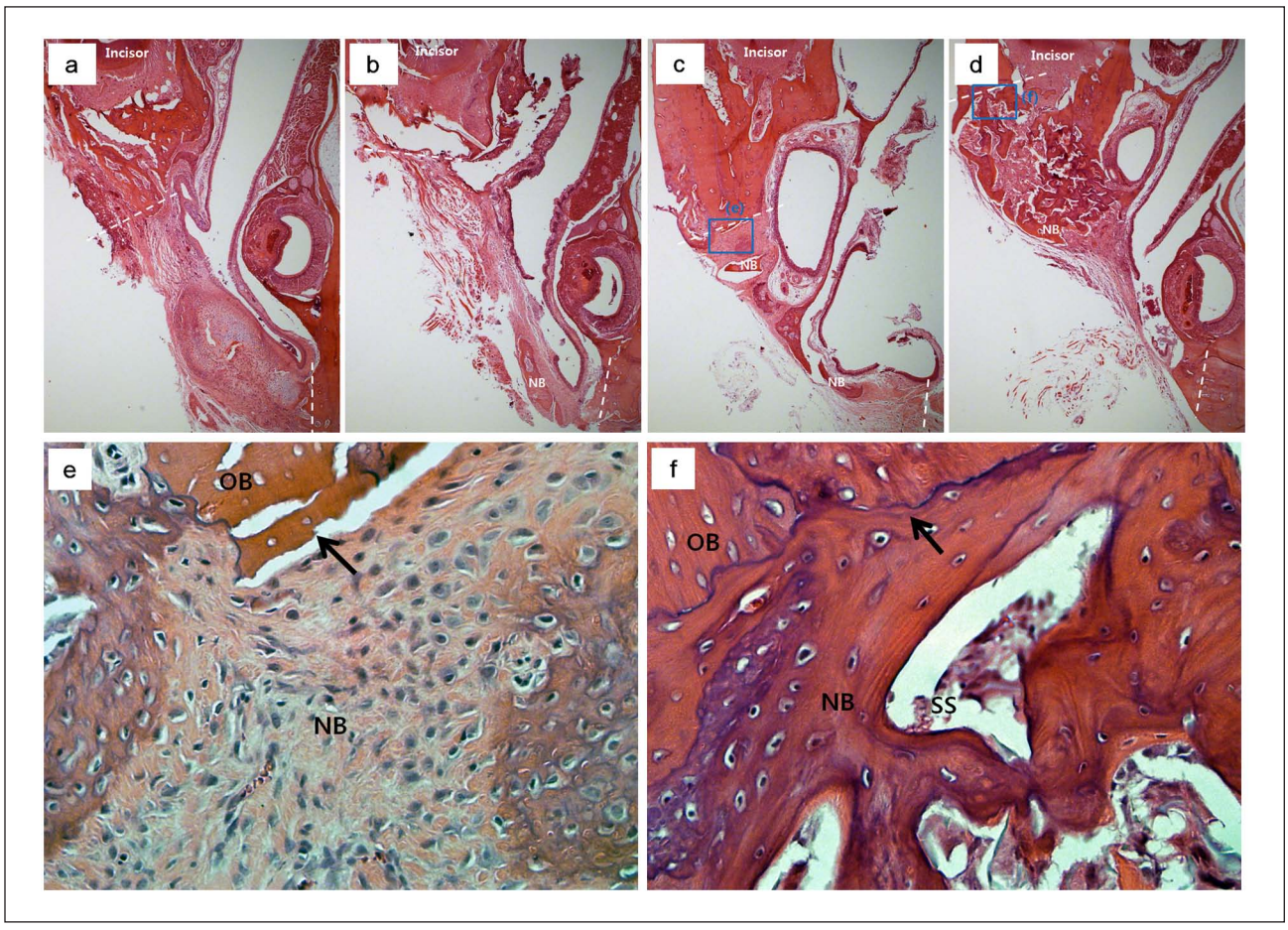

Figure 6. Representative histology images of hematoxylin and eosin (H&E) staining of new bone tissue formed within the defect at (a) 2 weeks, (b) 4 weeks, and (c) 6 weeks of the defect group and (d) 6 weeks of the silk-implanted group. Tissue in-growth and new bone formation increased with increasing test period. The silk scaffold implantation substantially improved the bone formation and showed almost complete defect closure (magnification ×40). Higher magnification (×400) of the H&E stained histology images; (e) control defect group at 6 weeks and (f) silk-implanted group at 6 weeks. New bone growing from the edge of the defect (arrow) is observed for both groups. While the empty defect group showed loosely organized nonwoven bone, the silk scaffold-implanted group showed lamellar-structured woven bone (arrows: defect margins, SS: silk scaffold, NB: new bone, and OB: old bone).

representative model of implantable biomaterials for bone regeneration. There was a gradual increase in bone healing over time; however, the healing was incomplete at 6 weeks as confirmed by μ-CT and histological analyses. Compared to the empty defect group, the silk scaffold group showed significantly enhanced bone formation. Specifically, the bone volume and healing of the area within the defect were significantly greater for the group which received a biomedical implant (silk scaffold) than for the control group. The silk scaffold is thus considered to provide effective scaffolding conditions for in vivo cellular in-growth and osteoconduction. In other words, the alveolar bone regeneration animal model evidenced the capacity of the silk scaffold to be potentially applicable for alveolar bone regeneration.

Like any model, this small animal procedure does not completely simulate the clinical alveolar bone defect and its healing conditions. However, it is a better representation than other bone defect models, such as those of the calvarium. The inexpensive nature and the technical simplicity extend the application of the new model of premaxillary bone defect to preclinical tests of developed biomaterials and tissue-engineered constructs.

Conclusion

A novel, reproducible, easily accessible, load-bearing, 4-mm semicircular, critical-sized premaxillary alveolar bone defect model was established modifying a GPP model in rats. Time-sequenced monitoring of the bone defect, with and without implantation of a silk scaffold, was performed using μ-CT and histological analyses to establish the model. This small animal model is suitable for extensive use as a preclinical platform for the development of biomaterials and tissue-engineered constructs for alveolar bone augmentation and sinus lifting in dental implantation.

Declaration of conflicting interests

The authors declare that there is no conflict of interest.

Funding

This study was supported by grants from the Priority Research Centers Program (2009-0093829), National Research Foundation, South Korea, and Department of Biotechnology, Govt of India.

References

1. Farré-Guasch E, Prins HJ, Overman JR, et al. Human maxillary sinus floor elevation as a model for bone regeneration enabling the application of one-step surgical procedures. *Tissue Eng Part B Rev* 2013; 19(1): 69–82.
2. Dunn CA, Jin Q, Taba M Jr, et al. BMP gene delivery for alveolar bone engineering at dental implant defects. *Mol Ther* 2005; 11(2): 294–299.
3. Conejero JA, Lee JA, Parrett BM, et al. Repair of palatal bone defects using osteogenically differentiated fat-derived stem cells. *Plast Reconstr Surg* 2006; 117(3): 857–863.
4. Hämmerle CH and Glauser R. Clinical evaluation of dental implant treatment. *Periodontol 2000* 2004; 34: 230–239.
5. Kim J-H, Kim MK, Park JH, et al. Performance of novel nanofibrous biopolymer membrane for guided bone regeneration within rat mandibular defect. *In Vivo* 2011; 25(4): 589–595.
6. Szpalski C, Barr J, Wetterau M, et al. Cranial bone defects—current and future strategies. *Neurosurg Focus* 2010; 29(6): E8.
7. Khanna-Jain R, Mannerström B, Vuorinen A, et al. Osteogenic differentiation of human dental pulp stem cells on β-tricalcium phosphate/poly (L-lactic acid/caprolactone) three-dimensional scaffolds. *J Tissue Eng* 2012; 3(1): 2041731412467998.
8. Bang SH, Kim T-H, Lee HY, et al. Nanofibrous-structured biopolymer scaffolds obtained by a phase separation with camphene and the initial cellular events. *J Mater Chem* 2011; 21: 4523–4530.
9. El-Bokle D, Smith SJ, Germane N, et al. New technique for creating permanent experimental alveolar clefts in a rabbit model. *Cleft Palate Craniofac J* 1993; 30(6): 542–547.
10. Griffioen FM, Smit-Vis JH and Urbanus NA. Facial growth in the rabbit after autologous grafting in unilateral clefts. *Cleft Palate J* 1988; 25(3): 226–234.
11. Haas R, Donath K, Födinger M, et al. Bovine hydroxyapatite for maxillary sinus grafting: comparative histomorphometric findings in sheep. *Clin Oral Implants Res* 1998; 9(2): 107–116.
12. Hochuli-Vieira E, Real Gabrielli MF, Garcia IR Jr, et al. Frontal sinus obliteration with heterogeneous corticocancellous bone versus spontaneous osteoneogenesis in monkeys (Cebus apella): histologic analysis. *J Oral Maxillofac Surg* 2003; 61(2): 214–221.
13. Wang Y, Shi B, Li Y, et al. Comparative study of maxillary growth and occlusal outcome after autogenous rib grafting in complete cleft palate defect. *J Craniofac Surg* 2006; 17(1): 68–79.
14. Schlegel KA, Rupprecht S, Petrovic L, et al. Preclinical animal model for de novo bone formation in human maxillary sinus. *Oral Surg Oral Med Oral Pathol Oral Radiol Endod* 2009; 108(3): e37–e44.
15. Mehrara BJ, Saadeh PB, Steinbrech DS, et al. A rat model of gingivoperiosteoplasty. *J Craniofac Surg* 2000; 11(1): 54–58.
16. Nguyen PD, Lin CD, Allori AC, et al. Establishment of a critical-sized alveolar defect in the rat: a model for human gingivoperiosteoplasty. *Plast Reconstr Surg* 2009; 123(3): 817–825.
17. Nguyen PD, Lin CD, Allori AC, et al. Scaffold-based rhBMP-2 therapy in a rat alveolar defect model: implications for human gingivoperiosteoplasty. *Plast Reconstr Surg* 2009; 124(6): 1829–1839.
18. Seoane J, López-Niño J, Tomás I, et al. Simulation for training in sinus floor elevation: new surgical bench model. *Med Oral Patol Oral Cir Bucal* 2012; 17(4): e605–e609.
19. Mandal BB and Kundu SC. A novel method for dissolution and stabilization of non-mulberry silk gland protein fibroin using anionic surfactant sodium dodecyl sulfate. *Biotechnol Bioeng* 2008; 99(6): 1482–1489.
20. Mandal BB and Kundu SC. Non-mulberry silk gland fibroin protein 3-D scaffold for enhanced differentiation of human mesenchymal stem cells into osteocytes. *Acta Biomater* 2009; 5(7): 2579–2590.
21. Patra C, Talukdar S, Novoyatleva T, et al. Silk protein fibroin from *Antheraea mylitta* for cardiac tissue engineering. *Biomaterials* 2012; 33(9): 2673–2680.
22. Mandal BB and Kundu SC. Cell proliferation and migration in silk fibroin 3D scaffolds. *Biomaterials* 2009; 30(15): 2956–2965.
23. Jang JH, Castano O and Kim H-W. Electrospun materials as potential platforms for bone tissue engineering. *Adv Drug Deliv Rev* 2009; 61(12): 1065–1083.
24. Lee HY, Jin GZ, Shin US, et al. Novel porous scaffolds of poly(lactic acid) produced by phase-separation using room temperature ionic liquid and the assessments of biocompatibility. *J Mater Sci Mater Med* 2012; 23(5): 1271–1279.
25. Lü K, Xu L, Xia L, et al. An ectopic study of apatite-coated silk fibroin scaffolds seeded with AdBMP-2 modified canine bMSCs. *J Biomater Sci Polym Ed* 2012; 23(1–4): 509–526.
26. Matic DB and Power SM. Evaluating the success of gingivoperiosteoplasty versus secondary bone grafting in patients with unilateral clefts. *Plast Reconstr Surg* 2008; 121(4): 1343–1353.
27. Freng A. Single layered periosteoplasty in experimental mid-palatal clefts: a histological study in the cat. *Scand J Plast Reconstr Surg* 1979; 13(3): 401–408.
28. Pearce AI, Richards RG, Milz S, et al. Animal models for implant biomaterial research in bone: a review. *Eur Cell Mater* 2007; 13: 1–10.
29. Estaca E, Cabezas J, Usón J, et al. Maxillary sinus-floor elevation: an animal model. *Clin Oral Implants Res* 2008; 19(10): 1044–1048.
30. Mills LA and Simpson AH. In vivo models of bone repair. *J Bone Joint Surg Br* 2012; 94(7): 865–874.
31. Diah E, Lo LJ, Yun C, et al. Cleft oronasal fistula: a review of treatment results and a surgical management algorithm proposal. *Chang Gung Med J* 2007; 30(6): 529–537.

32. Jackson IT, Moreira-Gonzalez AA, Rogers A, et al. The buccal flap—a useful technique in cleft palate repair? *Cleft Palate Craniofac J* 2004; 41(2): 144–151.
33. Li WJ, Laurencin CT, Caterson EJ, et al. Electrospun nanofibrous structure: a novel scaffold for tissue engineering. *J Biomed Mater Res* 2002; 60(4): 613–621.
34. Shin SH, Purevdorj O, Castano O, et al. A short review: recent advances in electrospinning for bone tissue regeneration. *J Tissue Eng* 2012; 3(1): 2041731412443530.
35. Park KE, Jung SY, Lee SJ, et al. Biomimetic nanofibrous scaffolds: preparation and characterization of chitin/silk fibroin blend nanofibers. *Int J Biol Macromol* 2006; 38(3–5): 165–173.